Inoue *et al. Earth, Planets and Space* (2022) 74:114
https://doi.org/10.1186/s40623-022-01673-8

Earth, Planets and Space

EXPRESS LETTER

Open Access

A broadband magnetotelluric survey for Mt. Meakandake volcano with special attention to the unrest during 2016–2017

Tomohiro Inoue[1*], Takeshi Hashimoto[2], Ryo Tanaka[2] and Yusuke Yamaya[3]

Abstract

We performed a broadband magnetotelluric (BBMT) survey and three-dimensional resistivity modeling for the Meakandake volcano in eastern Hokkaido, Japan, where remarkable ground deformation suggests a sill-like intrusion on the northeastern flank from 2016 to 2017. The volcano remained unerupted, and therefore the volcanological meaning of the deformation was unclear, making the evaluation of the "unrest" event difficult. Our 3D MT model has revealed a subvertical low-resistivity column C1 (approximately 1–10 Ωm) extending from 0.5 km BSL (below sea level) to a deeper part of Mt. Meakandake. The conductor C1 was not right on the presumed sill but just beneath the summit craters offset southwest. We performed a sensitivity test in which the bottom limit of C1 was varied, and confirmed that C1 was meaningful down to approximately 30 km BSL. The vertical reach in depth was necessary to reproduce the impedance phases out of quadrant at some sites west of Mt. Meakandake. In addition, we interpreted that the uppermost part of C1 was probably connected to the active vents of Mt. Meakandake through presumed subvertical pathways of heat and fluids, corresponding to the alignment of microearthquakes. On the other hand, we found no remarkable conductivity anomalies beneath the northeastern flank, where the sill-like inflation source was presumed. While our MT data do not suggest a thin sill at depth, it does not exclude the possibility that the ground inflation has been caused by a lateral magmatic or hydrothermal intrusion that branched from a certain depth of the subvertical conductor C1.

Keywords: Broadband magnetotelluric survey, Meakandake volcano, Magma plumbing system, 3D resistivity model

*Correspondence: tomohiro1832@eis.hokudai.ac.jp

[1] Department of Natural History Sciences, Graduate School of Science, Hokkaido University, N10W8, Kita-ku, Sapporo, Hokkaido 060-0810, Japan
Full list of author information is available at the end of the article

Graphical Abstract

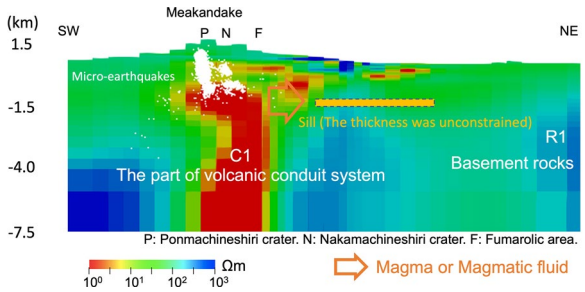

Introduction

Mt. Meakandake, located in the southwestern part of the Akan Caldera, is one of the active stratovolcanoes in eastern Hokkaido, northern Japan (Fig. 1). The volcanic cones composing Mt. Meakandake, such as Mt. Nakamachineshiri, Mt. Ponmachineshiri and Mt. Akanfuji were formed in sequence after 20 ka. The latest magmatic event was the scoria eruption that occurred at Ponmachineshiri crater at approximately 1 ka (Wada et al. 1998). In historic times, intermittent phreatic eruptions from the two craters (Ponmachineshiri and Nakamachineshiri: hereafter, P and N craters) were recorded between 1950 and 1966, followed by several phreatic eruptions at P crater in 1988, 1996, 1998, 2006 and 2008 (Japan Meteorological Agency (JMA) 2013). At present, some fumaroles and boiling ponds are seen at P and N craters. Steaming ground and hot springs are also seen at lower altitudes around the volcano. In particular, geothermal activities are noticeable in the central area between Mt. Meakandake and Mt. Oakandake. On the other hand, Mt. Oakandake has no eruptive activities confirmed in historic times, but weak geothermal activity is currently recognized (Tamada and Nakagawa 2009).

Remarkable ground inflation was observed by GNSS and InSAR on the northeastern foot of Mt. Meakandake from 2016 to 2017 (Geospatial Information Authority of Japan 2018). This inflation was presumed to be caused by a sill-like source at a depth of approximately 3 km in the middle of Mt. Meakandake and Mt. Oakandake, suggesting that magma accumulation may have occurred there (the red rectangle in Fig. 1; Faculty of Science, Hokkaido University 2019). However, the unrest event did not result in an actual eruption, and the relationship between the deformation and volcanic activity has been controversial. If the geometrical relationship between the magma plumbing system of the volcano and the ground deformation is imaged by geophysical exploration, it will be useful in evaluating the unrest event in relation to the volcanic activity including a future eruption.

Hasegawa et al. (2009) reported a gravity map of the Akan caldera by an extensive survey. They provided the general information on the caldera-scale structure including the basement level. Meanwhile, they found three low-gravity anomalies on the south side of Lake Akan, and interpreted that they correspond with the eruption centers of caldera-forming eruptions in the past.

The bulk electrical resistivity of a rock changes remarkably depending on the saturation of pore fluid as well as the temperature (Tyburczt and Waff 1983; Kariya and Shankland 1983; Nesbitt 1993). Hence, magnetotelluric (MT) sounding helps image the distribution of magma or hydrothermal water within a volcano. Many previous studies interpreted a low-resistivity body within a volcano as the path for volcanic fluids (e.g., Ogawa et al. 2014; Peacock et al. 2015; Matsunaga et al. 2020; Matsushima et al. 2020). In this way, magma or hydrothermal systems can often be imaged as low-resistivity anomalies by MT sounding.

In the 1990s, the New Energy and Industrial Technology Development Organization (NEDO) conducted an MT survey as a part of the Geothermal Development Promotion Survey (NEDO 1992), including drilling surveys at several sites on the eastern foot of Mt. Meakandake. The depth range of their MT model was about 4 km. On the southern shore of Lake Akan, Mogi et al. (2011) conducted an audio-frequency band magnetotelluric (AMT)/broadband magnetotelluric (BBMT) survey to investigate the geothermal system underlying the hot spring zone. This MT survey proposed a model in which low-density layers extending in the shallow part of the southern shore of Lake Akan mixes with ground water to form hot spring reservoirs. However, their survey area was offset northward from the deformation zone. More recently, an AMT survey was performed across the summit along a NE–SW direction as a part of the research for monitoring volcanic activity of Mt.

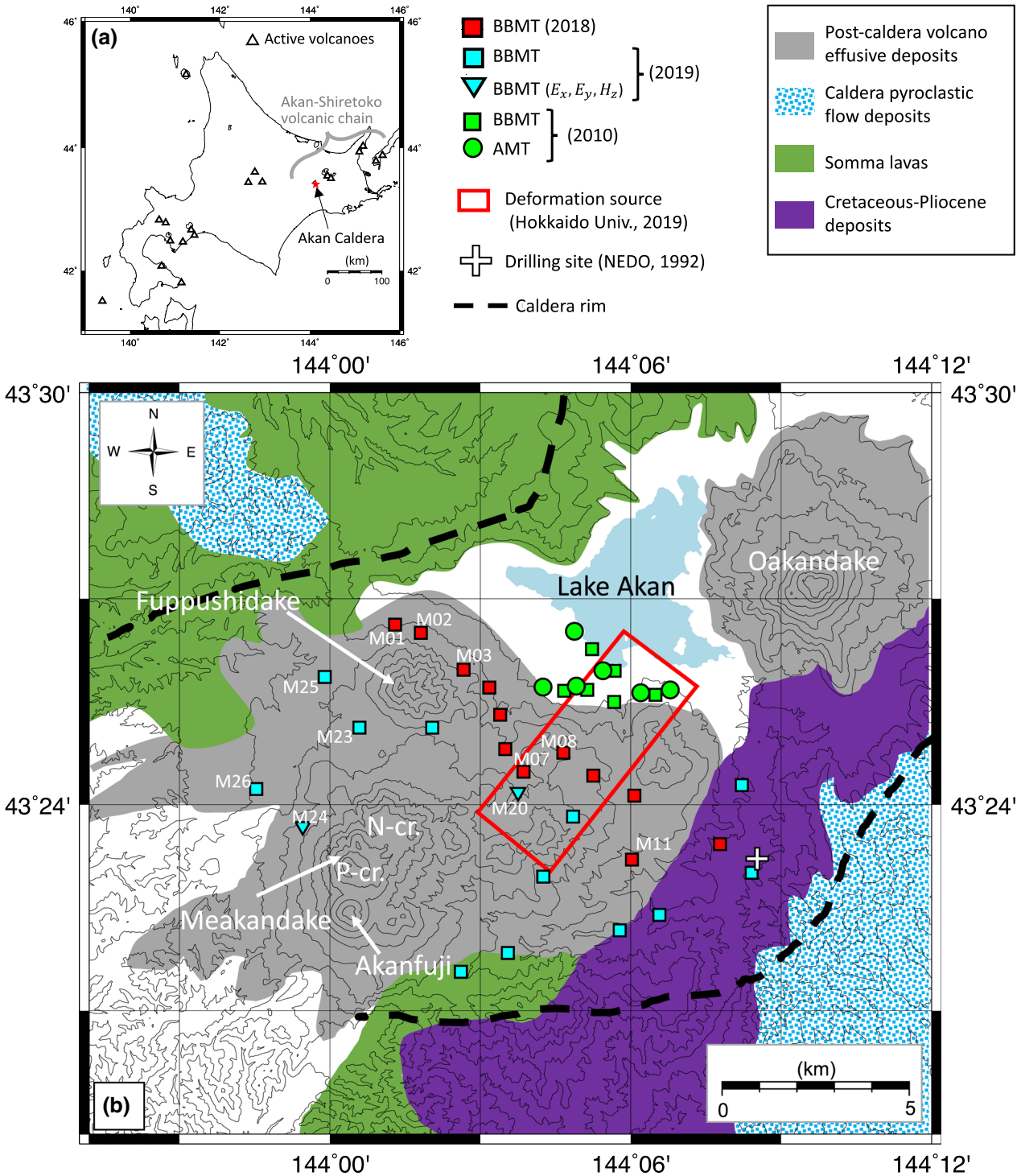

Fig. 1 **a** Location of Akan Caldera in Hokkaido, Japan. **b** Location of the MT sites in this study. The red rectangle indicates the sill-like source model of the ground deformation during 2016 and 2017 (Faculty of Science, Hokkaido Univ 2019). The simplified geological map is adapted from the report by Satoh (1965)

Meakandake (Takahashi et al. 2018). Takahashi et al. (2018) revealed the existence of the low-resistivity layers located about several hundred meters beneath the currently active craters (P and N) and a fumarolic area. These low-resistivity layers were interpreted in relation to the shallow hydrothermal system. The depth range was limited to approximately 2 km, and therefore, it is difficult to discuss the deeper plumbing system.

Therefore, we aimed to clarify the resistivity structure of Mt. Meakandake to greater depth and detail by performing an extended MT survey and 3D resistivity modeling. First, we conducted a BBMT survey around Mt. Meakandake, including the source region of the ground inflation during 2016–2017. We then performed a 3D inversion by combining the new data (2018 and 2019 survey) with AMT/BBMT data obtained on the southern shore of Lake Akan in 2010 (Mogi et al. 2011) to cover the whole of sill-like inflation source. In addition, we performed a sensitivity test to examine the uncertainties of the resistivity model. Furthermore, the magma plumbing system of Mt. Meakandake was evaluated based on our 3D resistivity model combined with other related information, such as the gravity anomaly, hypocenter distribution, drilling data, and previous MT surveys.

Magnetotelluric data in 2018 and 2019

From August to September in 2018 and 2019, we performed new BBMT campaigns in which we recorded naturally occurring variations in geomagnetic fields and associated induced electric fields at 26 sites using the Phoenix MTU-5A system (Fig. 1). The typical record duration at each site was three to seven days. We used Pb–$PbCl_2$ electrodes for the electric field and induction coils (MTC-50 and MTC-50H) for the magnetic field. The sites named M20 and M24 (Fig. 1) measured two components of electric fields and the vertical geomagnetic field only. The MT responses at these two sites were calculated using the horizontal geomagnetic field data at M22 or M25 (Additional file 1: Fig. S1) that were measured on the same days.

These time series data were converted into impedance tensors using the SSMT2000 software (Phoenix Geophysics Ltd.). To remove biases caused by local noise, remote reference processing (Gamble et al. 1979) was applied using the horizontal magnetic field at Sawauchi station (run by Nittetsu Mining Consultants Co., Ltd.), located approximately 550 km from our study area.

The sounding curves in the forms of apparent resistivity and phase that were calculated from the full impedance at three selected sites are shown in Fig. 2a. Responses at other sites are shown in the Additional file 1: Fig. S2. The impedance Z_{yx} phases are out of the ordinary quadrant (− 180° to − 90°) in the long period (approximately 500–3000 s) at some sites (M23, M24, M25, M26) in the western part of Mt. Meakandake (see > 1000 s in the phase of M25; Fig. 2a). Such an MT impedance phase that exceeds 90° or − 90° in off-diagonal components is termed as the anomalous phase and has been reported in previous studies in some other regions (e.g., Jones et al. 1988; Ichihara et al. 2013; Aizawa et al. 2014). Such anomalous phases out of quadrant have been explained, for example, by a subvertical conductive column with a deeper low-resistivity body (Aizawa et al. 2014) or strong 3D resistivity contrast (Piña-Varas and Dentith 2018). The anomalous phases in this study may also be explained by the mechanism of such kinds as shown in the later section.

The induction vectors (Parkinson 1962) and the phase tensor ellipses (Caldwell et al. 2004) are shown in Fig. 2b. The phase tensor is graphically represented by an ellipse with its principal axes indicating the electromagnetic strike or the orthogonal direction to the strike. As typically shown in the panels of 9 s and 108 s in Fig. 2b, the major axis of the phase tensor for these periods was mostly in a direction along NW–SE. The induction vectors for 9 and 108 s generally point to the southwest. However, those at 108 s, for the sites around Mt. Fuppushidake (e.g., M01 and M02) are different, implying strong local heterogeneity. The absolute values of the skew angle also tended to exceed 5° in the long period range (> 1 s), suggesting that the deep part of the Akan caldera is more heterogeneous than the shallow part. Therefore, 3D modeling was applied in this study.

Three-dimensional modeling

The inversion

1. We obtained the 3D resistivity model around Mt. Meakandake using the ModEM inversion code (Egbert and Kelbert 2012; Kelbert et al. 2014). In addition to the BBMT data described in the previous section, we also used BBMT/AMT data on the southern shore of Lake Akan obtained in 2010 (Mogi et al. 2011). The MT response functions (full impedance and full tipper) at 6–16 periods per station were used as input for the inversion. The error floor was set to 5% of the absolute values of both the impedance tensor and tipper. If the observation error was larger than the error floor, the actual error was used as the input. The total model space [1138 (x) × 1138 (y) × 1212 (z) km] was into 48 × 48 × 85 cells (Additional file 1: Fig. S1b). The central area, where the MT sites were located, was divided into cells with sides of 250–500 m, so that no single cell contained more than one observation point. The surrounding space was meshed into coarser cells, in which the width increased by double as we moved away from

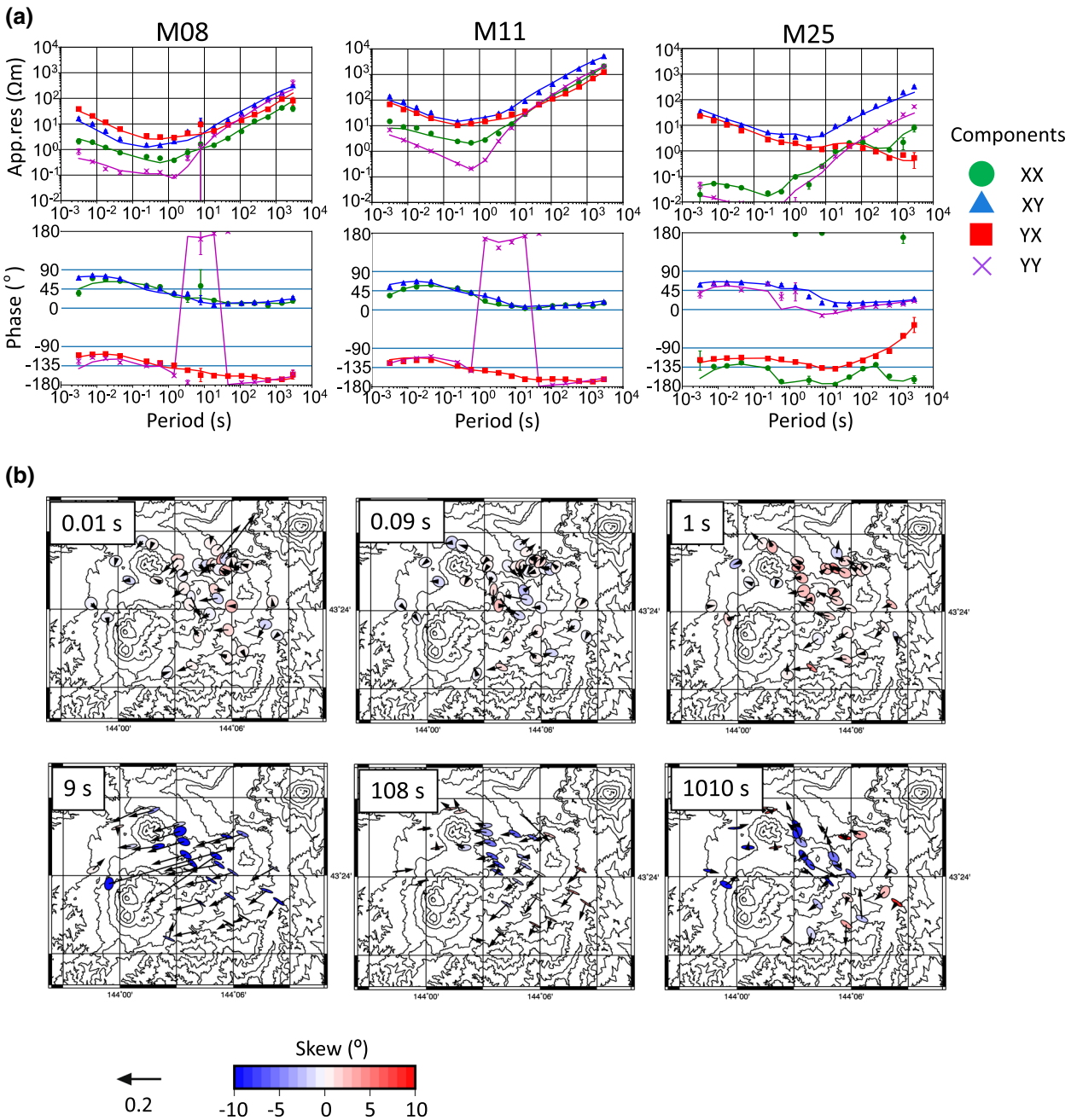

Fig. 2 **a** Apparent resistivities and phases at selected sites. The dots indicate the observed data, while the solid lines represent model response data from the optimal resistivity model shown in Fig. 3. **b** Induction vectors and the phase tensor ellipses. Ellipses were normalized by their major axis

the center. The vertical cell size was set to 25–50 m above sea level to reproduce the fine topography. From 0 to 4500 m BSL, a 50–500 m cells were introduced. Larger cells were modeled below 4500 m BSL. The resistivity model was started from a 100 Ωm uniform half space. The model included topography and bathymetry. The atmospheric and oceanic resistivities were fixed at 10^8 Ωm and 0.3 Ωm, respectively. The smoothing parameter was set uniformly at 0.4.

The RMS misfit between the observed and model responses converged to approximately 2.75 after 201 iterations. The model with the lowest RMS was adopted as the final model. The comparison between the observed

responses and the model responses calculated from the optimal model is shown in Fig. 2a and Additional file 1: Fig. S3. The data fit was generally good. In particular, the optimal model explained well the observations at the sites in the northeast and eastern foot of Mt. Meakandake (e.g., M08, M11). The anomalous phase of the Z_{yx} component on the western side of Mt. Meakandake (M23, M24, M25, M26) was also reproduced from the optimal model. On the other hand, slight inconsistencies were seen for the band from 1 to 10 s at some sites, such as M02, M03, M21 and M22 (Additional file 1: Fig. S2).

Figure 3a and b shows the horizontal and vertical cross sections of the final 3D resistivity model, respectively. Two distinct low-resistivity bodies were found below Mt. Meakandake and the north of Mt. Fuppushidake. One of the low-resistivity bodies of 1–10 Ωm (C1) emerged

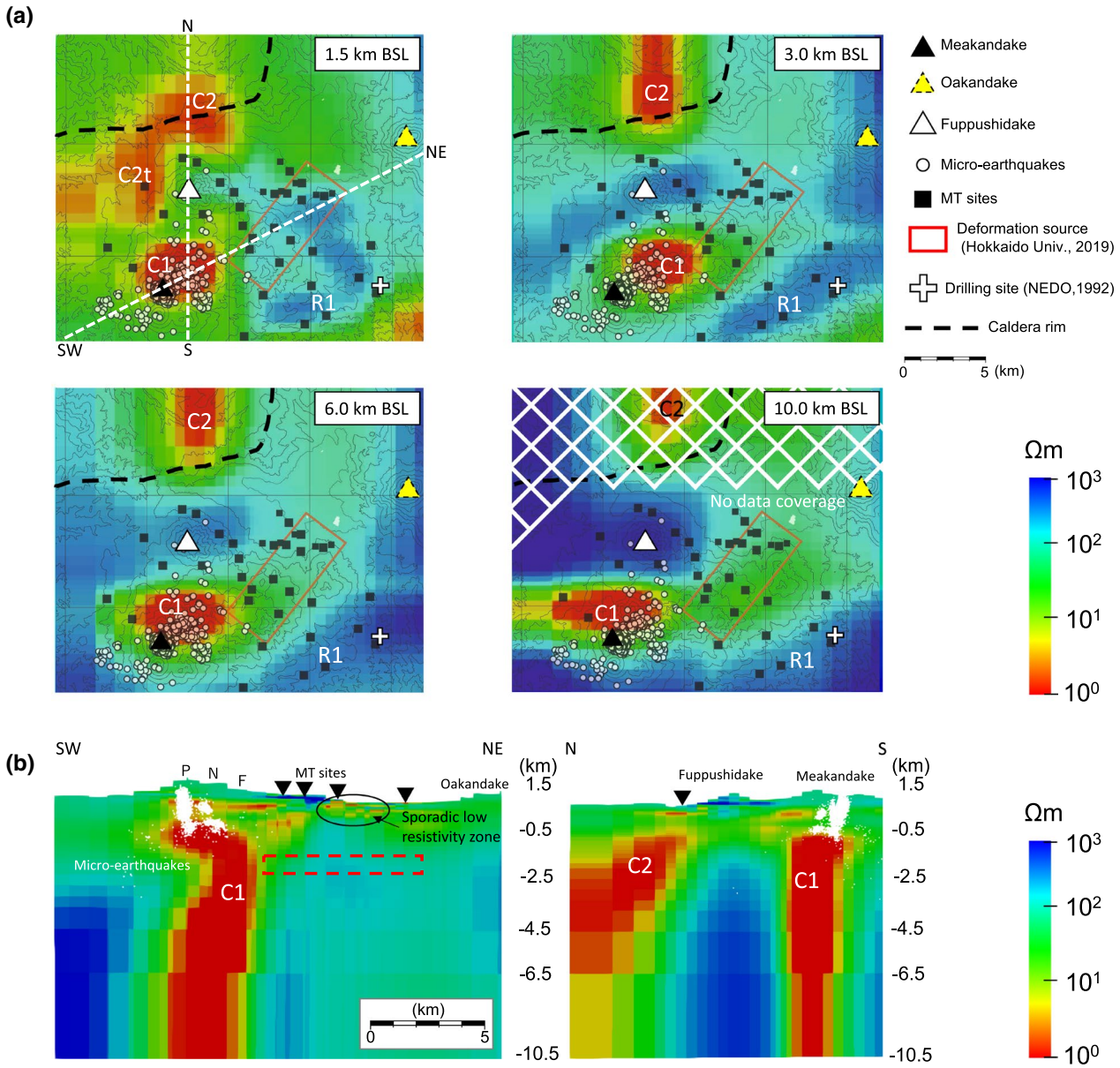

Fig. 3 **a** The final resistivity model sliced at 1.5, 3, 6 and 10 km BSL. Major features are labeled as C1, C2 and R1. **b** The resistivity model sliced along SW–NE and N–S lines, as shown in panel **a**. The red rectangles in panel **a** indicates the estimated deformation source by Faculty of Science, Hokkaido Univ. (2019). However, the source is shown by a dashed line in the cross section (**b**) as its thickness is unconstrained from the geodetic modeling. White dots indicate the hypocenters of volcanic earthquakes that occurred between 2004 and 2019 around Mt. Meakandake (provided by Sapporo Regional Headquarters, JMA). The symbols P, N, and F denote P and N craters, and a fumarolic area, respectively

from ca. 0.5 km BSL below Mt. Meakandake. In Fig. 3b, a structure shallower than 10 km was displayed, but the sensitivity tests in the following section required that C1 extended at least down to *ca.* 30 km deep. Separately from C1, the other low-resistivity body of approximately 1 Ωm (C2) was located from *ca*. 0.5 km BSL to *ca.* 15 km BSL on the northern side of Mt. Fuppushidake. As shown in the upper-left panel of Fig. 3a, a low-resistivity tongue (C2t) branching from C2 was found at 1.5 km BSL. On the other hand, no distinct low-resistivity body was found in the region where the 2016–2017 sill-like pressure source model was estimated (i.e., the northeastern flank of Mt. Meakandake at *ca.* 3 km depth; the red rectangle on Fig. 3). Instead, the sporadic low-resistivity zone below 10 Ωm appeared near the ground surface over the source region (Fig. 3b). In contrast to such low-resistivity anomalies, the region directly beneath Mt. Fuppushidake showed moderate-to-high resistivities without any notable features. Meanwhile, we found a broad high resistivity (R1) from Mt. Oakandake to the eastern flank of Mt. Meakandake, corresponding to the outer edge of the Akan caldera. In a shallow part (1.5 ~ 3.0 km BSL), R1 was bounded by another low-resistivity zone in the southeast, although the low-resistivity zone was located outside the observation area and the cell was coarse, so the detailed reality of the low-resistivity zone was unknown in this study.

Sensitivity tests

To verify how robust the structures of the main low-resistivity bodies C1 and C2 are in the optimal model obtained in this study, sensitivity tests were performed using the following procedure. First, we performed "total elimination" tests in which the resistivity values of the blocks corresponding to C1 and C2 of the optimal model were separately replaced by 20 Ωm, which was approximately the same as the ambient value. Then, we checked how the response curves (dashed lines in the left panels in Fig. 4a) of the modified models deviated from the observed data. In the second step, to confirm the significance of the bottom depth of the low-resistivity bodies in more detail, we separately performed the "partial-elimination" tests, where the resistivity of C1 and C2 below a certain depth ($D_{\max}$) was replaced by 20 Ωm, and calculated the model response at an effective site (M03 or M23, respectively) by varying $D_{\max}$ as 4.5, 21, 37, and 69 km BSL. The results are shown in the right panels in Fig. 4a and b.

In the first test, the RMS misfit of the "total eliminated models" for C1 and C2 was 5.95 and 4.25, respectively. As seen in the left panels of Fig. 4a and b, the response curves of these models deviated significantly from the observed data. Therefore, both C1 and C2 were required by the data. Since the RMS misfit of the optimal model was 2.75, the increment of misfit by eliminating C1 and C2 was 3.20 and 1.50, respectively, indicating that C1 was relatively more significant. It should be noted that the size of C2 has a great uncertainty because of no data coverage, as well as of a sudden jump in cell size near the anomaly, which potentially exaggerates stretching it out. Next, we took a closer look at the partial elimination tests. As shown in the right panel of Fig. 4a, neither of the models with C1 ranging down to 4.5 km or 21 km BSL could explain the anomalous phase that appeared in the Z_{yx} component at the relevant sites (M23, M24, M25, M26) on the western foot of Mt. Meakandake (RMS misfits were 5.59 and 3.78 for $D_{\max}=4.5$ and 21 km, respectively). At $D_{\max}=37$ km, the anomalous phase was explained. Bottom at 37 km satisfied only for the phase, and 69 km for both apparent resistivity and phase. However, the cell sizes in the between 37 and 69 km were relatively coarse (S5), and the mesh discretization issue remains. Therefore, it was difficult to mention the detailed length of C1. Considering the above, we concluded that the bottom depth of C1 must be at least *ca*. 30 km. We performed a similar test for C2. The RMS misfits were 3.48, 3.13, 2.80, and 2.76 for $D_{\max}=1.5$, 4.5, 9.5, and 12.5 km BSL, respectively. Considering the right panel of Fig. 4(b), although a large uncertainly remains regarding the shape of C2, we concluded that the bottom depth of C2 must be at least *ca*. 5 km BSL. In the same way, a sensitivity test was also performed on a low-resistivity anomaly C2t (Fig. 3a) located at 1.5 km BSL on the west side of C2. As a result, this low-resistivity feature was necessary to reproduce the induction vectors at the site located on the west side (e.g., M24, M25; Additional file 1: Fig. S3) for the period range from approximately 3 to 250 s.

Magma or hydrothermal reservoirs were considered as the candidates for the sill-like pressure source materials. If it is partial melts, the resistivity of a few tens of Ωm is reasonable (Gaillard 2004), and if it is hot saline water, the resistivity of several Ωm can be considered (Takakura 2000). Such a low-resistivity body (Ca) corresponding to a virtual magma or hydrothermal reservoir in the sill-like pressure source region was tested. Figure 4c shows the horizontal cross section of the model in which Ca, the low-resistivity brick referring to the sill-like pressure source (Faculty of Science, Hokkaido Univ. 2019), is placed. The top depth of Ca was fixed at 1.5 km BSL, but the thickness of the brick was varied. Figure 4d shows the response of each model for bulk resistivity values of 1 and 10 Ωm with varying thicknesses of 200 and 400 m. When the bulk resistivity of Ca was 10 Ωm, the RMS misfit was almost the same as that of the optimal model regardless of the thickness of Ca. In other words, the effect of Ca was not significant. When the bulk resistivity was

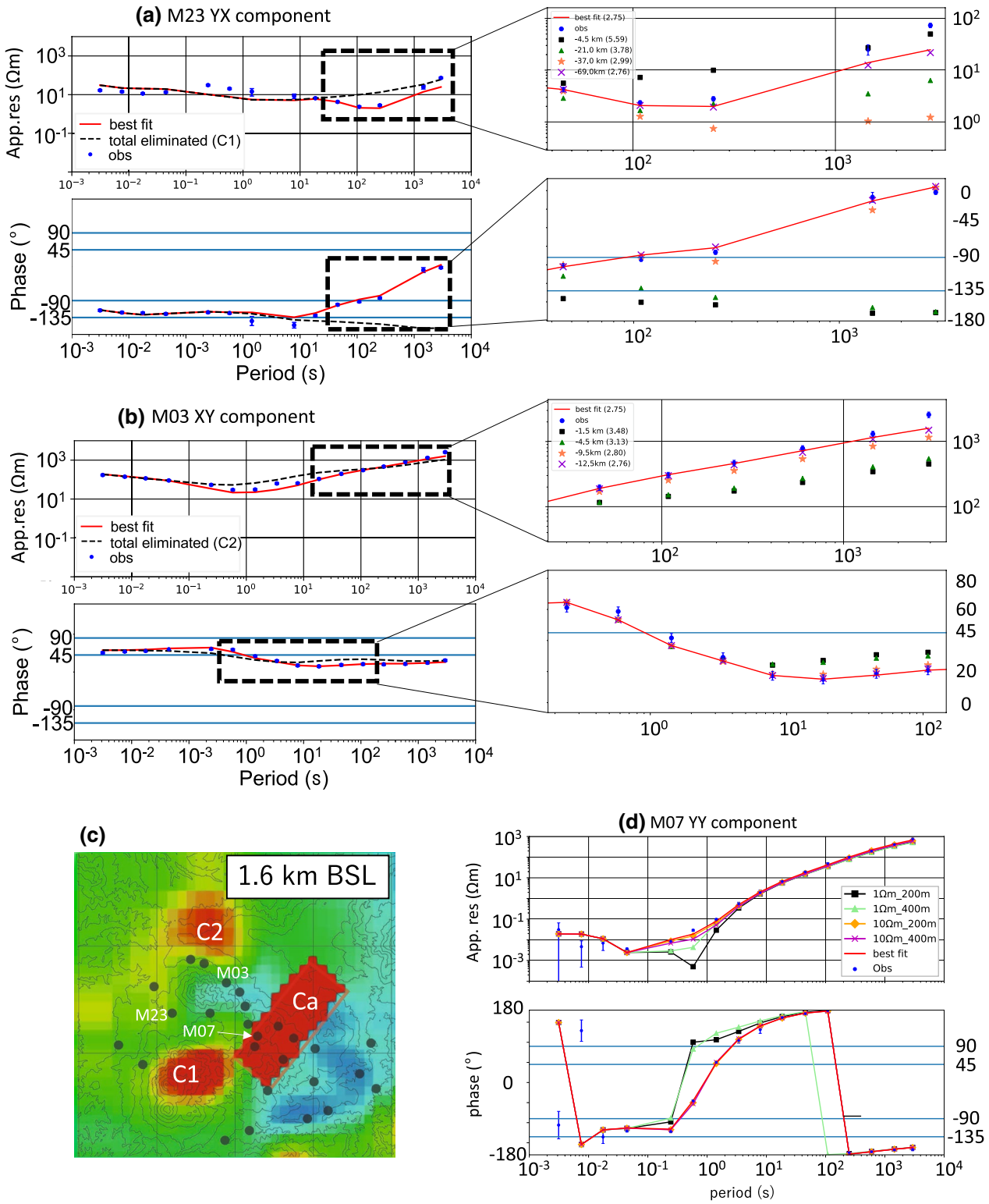

Fig. 4 **a** The response curves of the Z_{yx} component at site M23 when the lower limit of C1 was varied. **b** The response curves of the Z_{xy} component at site M03 when the lower limit of C2 was varied. Each symbol in the **a** and **b** represents the model response when D_{max} is varied. The values in parentheses are the RMS misfit values for the model. **c** The model with a thin conductive brick (Ca) corresponding to the sill-like pressure source (top depth at 1.5 km). **d** The response curves of the Z_{yy} component at site M07 when the bulk resistivity value and the thickness of Ca were varied

below 10 Ωm, the response curve started to deviate from the observed values. In particular, the deviation in the response curve appeared in the 0.1–10 s period band for the diagonal components of the impedance at sites on the northeastern foot of Mt. Meakandake (e.g., M07; Fig. 4d). The RMS misfit for the model with the bulk resistivity of Ca at 1 Ωm increased by 1.0 from the optimal model even with a thickness of 200 m.

Discussion

A possible link between the 2016–2017 deformation source and conduit system of the volcano

As mentioned previously, no distinct low-resistivity anomaly was imaged at a depth of approximately 3 km beneath the northeastern flank of Mt. Meakandake, where a sill-like deformation source was presumed (Fig. 3). As the result of the sensitivity test regarding Ca, the sites directly above the body (e.g., M08) are not significantly affected, but clear anomalies should appear at the sites on the edge of the body (e.g., M07). On the other hand, the observed data did not have such a feature, implying that nothing anomalous was there as the inversion model showed. However, if the body is thin in shape, or has an intermediate resistivity (several tens of Ωm), the possibility still remains that the body is a lateral intrusion. Several laboratory experiments on the resistivity of rocks in different temperature ranges have reported that partial melts exhibit resistivity values on the order of several Ωm to several tens of Ωm (e.g., Schilling et al. 1997; Gaillard 2004). According to Schilling et al. (1997), rock samples display resistivities above 10 Ωm when they contain silicate melt of 0.2 Ωm less than 5%. If it is a rhyolitic melt of 2–5% H_2O at 0.4 GPa, it can also be considered as the partial melt of 10 Ωm with the melt fraction of about 10–30% (Guo et al. 2016). Based on the discussion in the sensitivity test section, we consider that the reality of the deformation source may either be such a melt-poor mush magma or a more conductive thin magma sheet or hydrothermal fluid. We cannot distinguish them from our MT data because none of them have significant effects on the MT responses that we obtained at the ground surface.

As shown in Fig. 3, the hypocenters of volcanic microearthquakes occurring below Mt. Meakandake concentrate just under P and N craters. The lower limit of the hypocenter is almost coincident with the upper limit of C1. The microearthquakes appear to branch off from the top of C1 to the P and N craters (Fig. 3b). The lack of earthquakes in the interior of C1 suggests that brittle fracturing does not occur there, presumably because of high temperature or being already highly fractured (Hill et al. (2009) suggested the same idea at Mount St. Helens). Considering the geometry among C1, hypocenters and craters, it is probable that C1 corresponds to the conduit system of the volcano through which volcanic fluid and/or magma as well as heat are transported. We consider that hot volcanic fluid released from the uppermost part of C1 may cause microearthquakes on the way to the P and N craters. The deep low-frequency earthquakes (DLFE) occurring at 15–30 km right beneath Mt. Meakandake (JMA 2010) also imply that C1 corresponds to the conduit zone. However, the detailed relationship between C1 and DLFE remains unclear because of the coarse cell size at a depth of about 30 km in this resistivity model. The fact that the DLFE seem to occur in the deep part of (or below) C1 leads us to imagine a magmatic system. However, the tentative interpretations above need to be verified, especially in terms of the detailed geometry of C1, with additional field data and/or analyses in the future, since we currently lack sensitivity below a depth of 30 km and MT sites directly above the anomaly.

Comparison to gravity anomaly

High-resistivity belts (R1 in Fig. 3a) seem to correspond with the high gravity ridge along the southeastern part of the caldera rim (Hasegawa et al. 2009). The gravity high is probably related to the level of the basement rock of this area, which is considered to be relatively higher on the southeastern side of the caldera boundary (NEDO 1992). Therefore, we interpret that R1 corresponds to the basement rock of this area that mostly comprises Tertiary tuff breccia and welded tuff.

Some low-resistivity patches at approximately 1 Ωm are found at 0 km BSL on the southern shore of Lake Akan, as shown in Additional file 1: Fig. S7. This area is accompanied by two of the three gravity lows in the Bouguer anomaly map by Hasegawa et al. (2009). A geological study of Akan pyroclastic deposits by Hasegawa and Nakagawa (2007) suggests that Akan is a composite caldera resulting from multiple major eruptions. Hasegawa et al. (2009) pointed out that these low-gravity anomalies might be depressed craters associated with multiple caldera-forming eruptions infilled with low-density pyroclastic rocks. Roughly coincident locations and dimensions between the resistivity and gravity anomalies implies that these low-resistivity patches correspond to the low-density caldera infilling. However, to satisfy the resistivity value of *ca.* 1Ωm, we consider that the material should be either highly altered or saturated with saline water, suggesting a relation to the present hot springs on the lakeshore.

In addition, another low-resistivity patch C2t is found at approximately 1.5 km BSL on the west side of Mt. Fuppushidake (Fig. 3(a)). This is necessary to satisfy the direction and magnitude of the observed induction vectors for the period range from 3 to 250 s at MT sites located

on the west side (e.g., M02, M03, M24, M26). The C2t is coincident with the westmost gravity anomaly out of the three distinct anomalies in the Akan caldera (Hasegawa et al. 2009). Applying the same argument as the other two gravity lows, the abovementioned low-resistivity anomaly might also be related to caldera infilling in a presumed crater in the past. It is noteworthy that C2t seems to be connected to the deep-rooted northward-dipping conductive column C2 (Fig. 3), implying that another active magmatic system separated from C1. However, further detailed investigation and discussion should be a future work because C2 is imaged outside the measurement area of the present study and is not well constrained in terms of its geometry.

Comparison to borehole data

According to electrical logging by NEDO (1992), a low-resistivity layer of *ca.* 10 Ωm is found in the depth range from 450 to 550 m at the eastern foot of Mt. Meakandake. We compared our resistivity model with the well logs at the drilling site shown in Fig. 1 (Additional file 1: Fig. S8). They are in good agreement with each other. The depth range from 450 to 650 m at this location is classified as an altered layer with a high content of montmorillonite/chlorite (NEDO 1992). Montmorillonite is a clay mineral of the smectite series that is often found in hydrothermally altered strata and is known to have low resistivity (e.g., Takakura 2000; Komori et al. 2013). The clay-rich layer at this drilling site seems to have been produced by hydrothermal activities in the past because no significant surface geothermal anomalies are currently seen there. Meanwhile, our MT model shows a sporadic low-resistivity zone at approximately 1–10 Ωm in the shallow part above the 2016–2017 deformation source region at the northeastern foot of Mt. Meakandake (left panel in Fig. 3b). Geothermal manifestations, such as natural hot springs and fumarolic zones, are seen in this area. Therefore, it is likely that the low resistivity in this area corresponds to an altered montmorillonite-bearing layer due to pre-existing and ongoing hydrothermal activity.

The conceptual model of Mt. Meakandake

Based on the discussion thus far, we proposed the following conceptual model beneath the volcano, as shown in Fig. 5. According to our 3D resistivity model, low-resistivity layers (1–10 Ωm) lie in the shallow part beneath the active craters (P and N) (Fig. 3b), steaming ground in the middle (F), and the northeastern foot of the volcano. The low-resistivity layers (3–10 Ωm) beneath P, N, and F reported from the AMT survey in Takahashi et al. (2018) are plausibly the same as those we detected (Fig. 3(b); the depth of about 0 km). Takahashi et al (2018) considered that these low-resistivity layers (C1, C2, and C3 in Fig. 15 of the reference, corresponding to P, N, and F, respectively) are either the hydrothermal reservoir or hydrothermal alteration zones containing clay and hot water. The 2D resistivity section of Takahashi et al (2018) extends to a depth of about 2 km, and the equivalent of conductive layers in this study did not appear. Our MT survey has revealed that they are underlain by a distinct conductive column C1 that is probably rooted by a magmatic system that supplies heat and gases upward (Fig. 5). In this context, we

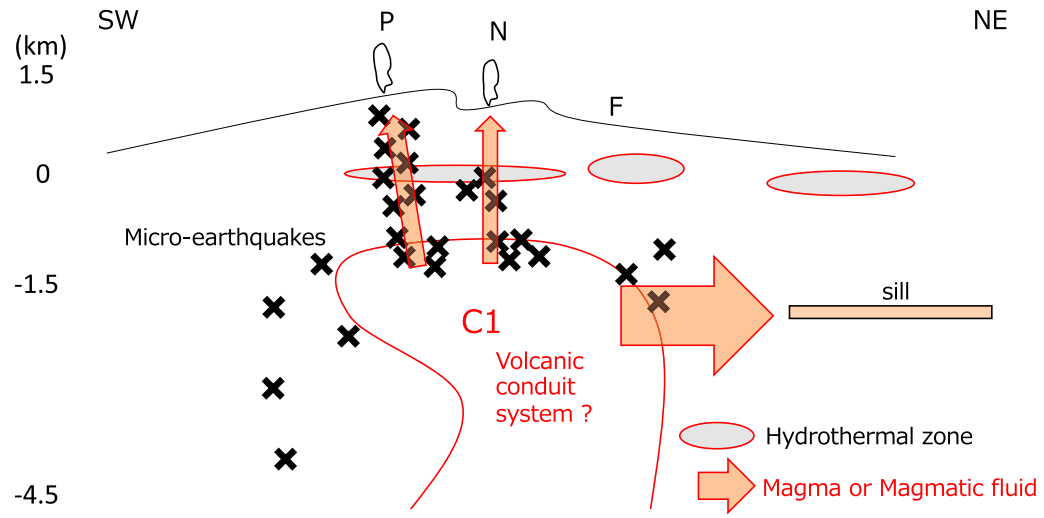

Fig. 5 Conceptual model of the shallow volcanic system of Mt. Meakandake based mainly on our MT model. Crosses indicate microearthquakes. P and N craters are indicated by P and N, respectively. The geothermal area with steaming ground in the middle of the NE flank is shown as F

agree with the interpretation by Takahashi et al. (2018) that attributed the shallow conductive features to the hydrothermal system. Meanwhile, our MT model does not exclude the existence of a magma sheet in the source region of the 2016–2017 deformation. If this is the case, we suggest that the magma was branched off from the upper part of C1 northeastward to pressurize a sill causing the deformation (Fig. 5).

Conclusion

We conducted a broadband MT survey at 26 sites on and around Mt. Meakandake volcano. Combining our data with the BBMT/AMT data obtained in 2010 (Mogi et al. 2011), a 3D resistivity model was obtained. One of the distinct resistivity anomalies was the highly conductive column C1 just beneath Mt. Meakandake. The correspondence between the lower limit of the microearthquakes and the top of C1 suggested a nonbrittle nature due to high temperatures or fractured conditions within C1, working as the pathway(s) of magma and volatiles. We considered that C1 and the currently active craters are connected with subvertical pathways along which microearthquakes were located.

On the other hand, no significant low-resistivity anomaly was detected in the 2016–2017 deformation source region from our inversion model. Meanwhile, the sensitivity test with forward modeling showed that neither a melt-poor magma chamber with a bulk resistivity greater than 10 Ωm nor even a magma sheet thinner than 200 m significantly affected the MT responses on the ground. In other words, the presence of such partial melt bodies in the deformation source region did not contradict our MT model. Although it is not constrained by the data, we suspected that the 2016–2017 unrest deformation was a lateral magma intrusion branching off from the upper part of conductive column C1. Additional MT measurements immediately above and west to south of C1 will constrain the anomaly better. Other sounding methods, such as seismic attenuation, will help to confirm the provisional interpretations that we proposed in this study.

Abbreviations

BBMT: Broadband magnetotelluric; BSL: Below sea level; ka: Kilo annum; JMA: Japan Meteorological Agency; NEDO: New Energy and Industrial Technology Development; AMT: Audio-frequency band magnetotelluric.

Supplementary Information

The online version contains supplementary material available at https://doi.org/10.1186/s40623-022-01673-8.

Additional file 1: We modified S6 caption of additional file. We uploaded the modified file (Additional_file_1_ESM.docx).

Acknowledgements

We are grateful to Prof. S. Sakanaka of Akita University for instrumental support. We thank Nittetsu Mining Consultants Co. Ltd. for providing us with reference geomagnetic data from the Sawauchi MT station. R. Ito and Y. Iwama are acknowledged for their assistance in the fieldwork. The hypocenter data were provided by the Sapporo Regional Headquarters, JMA. The 500 m mesh bathymetry model of the Japan Coast Guard was used for the 3D inversion. We gratefully thank three anonymous reviewers and the editor for their valuable comments. Generic Mapping Tools software (Wassel and Smith, 1998) was used to draw the figures in this study. This work was supported by JST SPRING, Grant Number JPMJSP2119.

Author contributions

TI and TH contributed to MT observations in 2018 and in 2019. TI, TH and RT analyzed data. YY acquired and analyzed the MT data in 2010 MT data. All authors contributed to the interpretation and approved the final manuscript. All authors read and approved the final manuscript.

Funding

This research was supported by Faculty of Science, Hokkaido University, Japan.

Availability of data and materials

MT data are available from Tomohiro Inoue on reasonable request.

Declarations

Ethics approval and consent to participate

Not applicable.

Consent for publication

Not applicable.

Competing interests

The authors declare that they have no competing interests.

Author details

[1]Department of Natural History Sciences, Graduate School of Science, Hokkaido University, N10W8, Kita-ku, Sapporo, Hokkaido 060-0810, Japan. [2]Institute of Seismology and Volcanology, Faculty of Science, Hokkaido University, N10W8, Kita-ku, Sapporo, Hokkaido 060-0810, Japan. [3]Renewable Energy Research Center, National Institute of Advanced Industrial Science and Technology (AIST), Machikedai 2-2-9, Koriyama, Fukushima 963-0928, Japan.

Received: 25 November 2021 Accepted: 5 July 2022
Published online: 25 July 2022

References

Aizawa K, Koyama T, Hase H, Uyeshima M, Kanda W, Utsugi M, Yoshimura R, Yamaya Y, Hashimoto T, Yamazaki K, Komatsu S, Watanabe A, Miyakawa K, Ogawa Y (2014) Three-dimensional resistivity structure and magma plumbing system of the Kirishima Volcanoes as inferred from broadband magnetotelluric data. J Geophys Res Solid Earth 119:198–215. https://doi.org/10.1002/2013JB010682

Caldwell TG, Bibby HM, Brown C (2004) The magnetotelluric phase tensor. Geophys J Int 158:457–469. https://doi.org/10.1111/j.1365-246X.2004.02281.x

Egbert GD, Kelbert A (2012) Computational recipes for electromagnetic inverse problems. Geophys J Int 189:251–267. https://doi.org/10.1111/j.1365-246X.2011.05347.x

Gaillard F (2004) Laboratory measurements of electrical conductivity of hydrous and dry silicic melts under pressure. Earth Planet Sci Lett 218(1–2):215–228. https://doi.org/10.1016/S0012-821X(03)00639-3

Gamble TD, Goubau WM, Clarke J (1979) Magnetotellurics with a remote magnetic reference. Geophysics 44:53–68. https://doi.org/10.1190/1.1440923

Guo X, Zhang L, Behrens H, Huaiwei N (2016) Probing the status of felsic magma reservoirs: constraints from the P-T-H_2O dependences of electrical conductivity of rhyolitic melt. Earth Planets Space Letters 443:54–62. https://doi.org/10.1016/j.epsl.2015.10.036

Hasegawa T, Nakagawa M (2007) Stratigraphy of Early to Middle Pleistocene pyroclastic deposits around Akan caldera, eastern Hokkaido, Japan. J Geol Soc Jpn 113:53–72. https://doi.org/10.5575/geosoc.113.53
Hasegawa T, Yamamoto A, Kamiyama H, Nakagawa M (2009) Gravity structure of Akan composite caldera, eastern Hokkaido, Japan: application of lake water corrections. Earth Planets Space 61:933–938. https://doi.org/10.1186/BF03353205
Hill GJ, Caldwell TG, Heise W, Chertkoff DG, Bibby HM, Burgess MK, Cull JP, Cas RAF (2009) Distribution of melt beneath Mount St Helens and Mount Adams inferred from magnetotelluric data. Nat Geosci 2:785–789. https://doi.org/10.1038/ngeo661
Ichihara H, Mogi T, Yamaya Y (2013) Three-dimensional resistivity modelling of a seismogenic area in an oblique subduction zone in the western Kurile arc: constraints from anomalous magnetotelluric phases. Tectonophysics 603:114–122. https://doi.org/10.1016/j.tecto.2013.05.020
Jones AG, Kurtz RD, Oldenburg DW, Boerner DE, Ellis R (1988) Magnetotelluric observations along the lithoprobe southeastern Canadian Cordilleran transect. Geophys Res Letter 15:677–680. https://doi.org/10.1029/GL015i007p00677
Kariya KA, Shankland TJ (1983) Electrical conductivity of dry lower crustal rocks. Geophysics 48:52–61. https://doi.org/10.1190/1.1441407
Kelbert A, Meqbel N, Egbert GD, Tandon K (2014) ModEM: a modular system for inversion of electromagnetic geophysical data. Comput Geosci 66:40–53. https://doi.org/10.1016/j.cageo.2014.01.010
Komori S, Kagiyama T, Takakura S, Ohsawa S, Mimura M, Mogi T (2013) Effect of the hydrothermal alteration on the surface conductivity of rock matrix: comparative study between relatively-high and low temperature hydrothermal systems. J Volcanol Geoth Res 264:164–171. https://doi.org/10.1016/j.jvolgeores.2013.08.009
Matsunaga Y, Kanda W, Takakura S, Koyama T, Saito Z, Seki K, Suzuki A, Kishita T, Kinoshita Y, Ogawa Y (2020) Magmatic hydrothermal system inferred from the resistivity structure of Kusatsu-Shirane Volcano. J Volcanol Geoth Res 390:106742. https://doi.org/10.1016/j.jvolgeores.2019.106742
Matsushima N, Utsugi M, Takakura S, Yamasaki T, Hata M, Hashimoto T, Uyeshima M (2020) Magmatic-hydrothermal system of Aso Volcano, Japan, inferred from electrical resistivity structures. Earth Planets Space 72:57. https://doi.org/10.1186/s40623-020-01180-8
Nesbit BE (1993) Electrical resistivity of crustal fluids. J Geophys Res Solid Earth 98:4301–4310. https://doi.org/10.1029/92JB02576
Ogawa Y, Ichiki M, Kanda W, Mishina M, Asamori K (2014) Three-dimensional magnetotelluric imaging of crustal fluids and seismicity around Naruko volcano, NE Japan. Earth Planets Space 66:158. https://doi.org/10.1186/s40623-014-0158-y
Parkinson WD (1962) The influence of continents and oceans on geomagnetic variations. Geophys J Int 6:441–449. https://doi.org/10.1111/j.1365-246X.1962.tb02992.x
Peacock JR, Mangan MT, McPhee D, Ponce DA (2015) Imaging the magmatic system of Mono Basin, California, with magnetotellurics in three dimensions. J Geophys Res Solid Earth 120:7273–7289. https://doi.org/10.1002/2015JB012071
Piña-Varas P, Dentith M (2018) Magnetotelluric data from the Southeastern Capricorn Orogen, Western Australia: an example of widespread out-of-quadrant phase responses associated with strong 3-D resistivity contrasts. Geophys J Int 212:1022–1032. https://doi.org/10.1093/gji/ggx459
Schilling FR, Partzsch GM, Brasse H, Schwarz G (1997) Partial melting below the magmatic arc in the central Andes deduced from geoelectromagnetic field experiments and laboratory data. Phys Earth Planet Int 103(1–2):17–31. https://doi.org/10.1016/S0031-9201(97)00011-3
Takahashi K, Takakura S, Matsushima N, Fujii I (2018) Relationship between volcanic activity and shallow hydrothermal system at Meakandake volcano, Japan, inferred from geomagnetic and audio-frequency magnetotelluric measurements. J Volcanol Geoth Res 349:351–369. https://doi.org/10.1016/j.jvolgeores.2017.11.019
Takakura S (2000) Relationship of resistivity to physical, chemical and mechanical properties of clay-bearing samples. Geophys Explor (butsuri-Tansa) 53(5):415–426
Tamada J, Nakagawa M (2009) Eruption history of Oakan volcano, eastern, Hokkaido Japan. Volcanol Soc Jpn. 54:147–162. https://doi.org/10.18940/kazan.54.4_147
Tyburczy JA, Waff HS (1983) Electrical conductivity of molten basalt and andesite to 25 kilobars pressure: geophysical significance and implications for charge transport and melt structure. J Geophys Res Solid Earth 88:2413–2430. https://doi.org/10.1029/JB088iB03p02413
Wada K, Ikegami H, Inaba T (1998) Chemical Compositions of the Rocks from Me-akan Volcano, Eastern Hokkaido, Japan: compositional Variety of Eruptive Magmas. Reports Taisetsuzan Inst Sci 32:43–60
Wessel P, Smith WHF (1998) New, improved version of generic mapping tools released. EOS Trans Am Geophys U 79(47):579. https://doi.org/10.1029/98EO00426
Faculty of Science, Hokkaido University (2019) Research report on volcanoes in Hokkaido (Mt. Meakandake) 1–74
Geospatial Information Authority of Japan (2018) Crustal Deformations around Meakan Volcano, Report of the Coordinating Committee for Prediction of Volcanic Eruptions, 128: 5–19
Japan Meteorological Agency (2010) The eruption of the Meakandake Volcano on November 2008, Report of Coordinating Committee for Prediction of Volcanic Eruption, 102: 1–15
Japan Meteorological Agency (Ed) (2013) National Catalogue of the Active Volcanoes in Japan, 4th ed Japan Meteorological Agency, Tokyo, p. 1498
Mogi T, Yamaya Y, Hashimoto T, Akita F, Shibata T, Takahashi T, Tamura S (2011) MT survey in Akanko Hot Springs, the proceedings of Society of Exploration Geophysicists of Japan, 125: 147–150
New Energy and Industrial Technology Development Organization (1992) Report of the Geothermal Development Promotion Survey (Akan), pp. 171–172, pp. 451–452, pp. 645–646
Satoh H (1965) Explanatory text of the geological map of Japan, scale 1: 50,000, Akanko, Kushiro, No. 7, Geological Survey of Japan

Publisher's Note